HAL
open science

The initial stages of heavy-ion collisions in the Color Glass Condensate framework

François Gelis

To cite this version:

François Gelis. The initial stages of heavy-ion collisions in the Color Glass Condensate framework. Pramana - Journal of Physics, 2015, 84 (5), pp.685-701. cea-01004418

HAL Id: cea-01004418

https://cea.hal.science/cea-01004418v1

Submitted on 8 Apr 2019

HAL is a multi-disciplinary open access archive for the deposit and dissemination of scientific research documents, whether they are published or not. The documents may come from teaching and research institutions in France or abroad, or from public or private research centers.

L'archive ouverte pluridisciplinaire **HAL**, est destinée au dépôt et à la diffusion de documents scientifiques de niveau recherche, publiés ou non, émanant des établissements d'enseignement et de recherche français ou étrangers, des laboratoires publics ou privés.

arXiv:1312.5497v2 [hep-ph] 23 Dec 2013

PRAMANA
— journal of
physics

© Indian Academy of Sciences

The initial stages of heavy-ion collisions in the Color Glass Condensate framework

FRANÇOIS GELIS[a, *]
[a]Institut de Physique Théorique, CEA Saclay, 91191 Gif sur Yvette cedex, France

Abstract. In this short review, we present the description of the early stages of a heavy ion collision at high energy in the Color Glass Condensate framework.

Keywords. Heavy ion collisions, Quantum Chromodynamics, Color Glass Condensate

PACS Nos.

1. Introduction

Heavy ion collisions at ultra-relativistic energies are used as a way to study in the laboratory the properties of nuclear matter in extreme conditions of temperature and density, where it is expected to undergo a transition to a deconfined state called the quark-gluon plasma [1]. In such a collision, one can distinguish several stages, illustrated in the figure 1, from the initial impact between the two nuclei to the final freeze-out after which the produced particles stop interacting. As the matter formed in the collision evolves, it

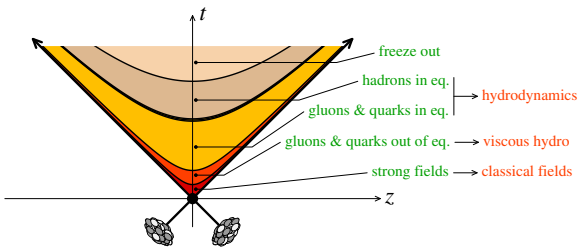

Figure 1. Successive stages of a heavy ion collision.

expands and cools down, which also implies that the strong coupling constant becomes progressively larger. Therefore, only the first stages (the impact itself, and shortly afterwards) stand a chance to be amenable to a description in terms of perturbative Quantum Chromo-Dynamics (QCD). The bulk evolution of the system during the subsequent stages is well described by means of transport models such as relativistic hydrodynamics [2–9], that only borrow a few inputs from QCD, in the form of transport coefficients and initial

*francois.gelis@cea.fr

conditions. The aim of this review is to discuss our present understanding of the QCD description of the early stages of heavy ion collisions, up to the stage where the hydrodynamical description may become applicable.

2. Gluon saturation, McLerran-Venugopalan model

In fact, the application of QCD to the study of heavy ion collisions faces two difficulties. Firstly, it is not at all obvious that the problem of calculating the bulk properties of the produced quarks and gluons can be treated by perturbative techniques. Indeed, most of the partons produced in such a collision are much softer than the collision energy itself. For a perturbative approach to be possible, one needs to justify that these partons are produced with a typical momentum much larger than the QCD non-perturbative scale $\Lambda_{\rm QCD}$. The second difficulty is that the parton density in nucleons becomes very large at high energy, as shown in the figure 2 (the longitudinal momentum fraction x is inversely proportional to the nucleon energy). When the occupation number in the projectiles ap-

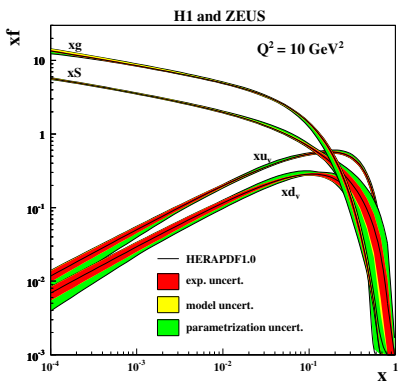

Figure 2. Parton distributions in a proton. From [10].

proaches the inverse of the coupling constant, the calculation of transition amplitudes becomes non-perturbative and cannot be done with the standard perturbative techniques. The difference between the dilute (left) and dense (right) regimes is illustrated in the figure 3. At high density, processes initiated by more than two partons become important

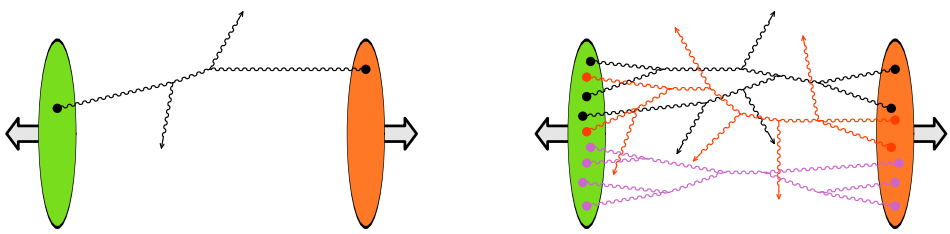

Figure 3. Typical process in a nucleus-nucleus collision. Left: dilute regime. Right: dense regime.

(the power counting relevant for this regime will be discussed in detail later), and multiple

disconnected subprocesses can occur simultaneously.

These two difficulties are in fact intimately related: the non-linear corrections that become important in the dense regime lead to the dynamical generation of a characteristic momentum scale –called the saturation momentum, denoted Q_s– proportional to the gluon density. The saturation momentum increases with the gluon density, and therefore with the collision energy, and at sufficiently high energy it is much larger than $\Lambda_{\rm QCD}$, justifying a weak coupling treatment. It owes its name to the fact that these non-linear effects tend to limit –to saturate– the growth of the gluon occupation number once it reaches values of order α_s^{-1}. Since the relevant density is the surface density, i.e. integrated over the collision direction, the saturation momentum also increases like the radius of the nucleus under consideration, proportional to the third power of the atomic number, $A^{1/3}$. The variations of Q_s with A and with the momentum fraction x are represented in the figure 4. For lead nuclei ($A \sim 200$) at LHC energy (i.e. $x \sim 10^{-4}$), the value of Q_s^2 is in the

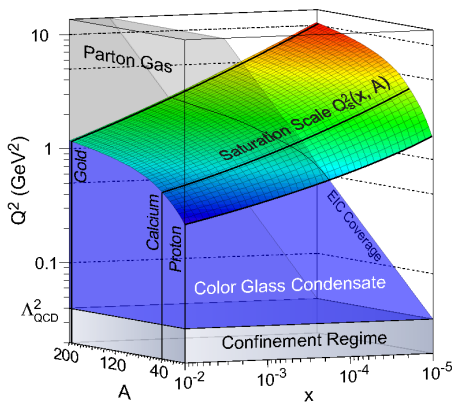

Figure 4. Saturation domain as a function of x and A. From [11].

range $2-4$ GeV^2, which should be sufficiently above $\Lambda_{\rm QCD} \approx 200$ MeV to justify a weak coupling expansion.

The concept of gluon saturation goes back to the early 80's [12–14]. Later on, these ideas were implemented in the McLerran-Venugopalan model [15–17], in which the fast partons are described as classical color sources moving on the light-cone, while the slower partons (mostly gluons) are described in terms of ordinary quantum fields. It is thus described by the following effective Lagrangian,

$$\mathcal{L} \equiv -\frac{1}{4} F_{\mu\nu} F^{\mu\nu} + J_\mu A^\mu \ , \tag{1}$$

where J_μ is the color current carried by the fast partons. In the case of the collision between two hadrons or nuclei, this current is the sum of two terms, representing color charges moving in opposite directions. There is an implicit cutoff Λ that separates the fast from the slow partons, depending on their longitudinal momentum. These color sources are static, because the transverse motion of the color charges inside the wave function of the projectiles is considerably slowed down by time dilation, and they appear as frozen during the short duration of the collision. In a given collision, J^μ is a snapshot of the transverse position of the color charges inside the projectiles. As a consequence, it cannot be known deterministically, and one can only hope to have a probability distribution for

J, usually denoted $W[J]$. Observables should be calculated for an arbitrary J, and then averaged over this probability distribution.

When this formalism is applied to the study of a collision, the initial state of the system is the "vacuum", since the two projectiles are entirely encoded in the current J_μ. Thus, to compute the expectation value of an observable $\widehat{\mathcal{O}}$, one must in fact evaluate $\langle 0_{\rm in}|\widehat{\mathcal{O}}|0_{\rm in}\rangle$ in the quantum field theory described by eq. (1). The best tool to organize the calculation of this type of matrix element is the Schwinger-Keldysh formalism [18, 19] (that can also been viewed in this context as a realization of Cutkosky's cutting rules [20, 21]).

In the saturated regime, the color current J is of order $Q_s^3 g^{-1}$ (the factor Q_s^3 just sets the correct dimension). The inverse power of the coupling, g^{-1}, is due to the fact that the occupation number (quadratic in J) is of order g^{-2} in the saturated regime. This factor deeply alters the power counting when applying this effective description to the calculation of observables. In order to see this, consider any connected subgraph of the diagram shown in the right panel of the figure 3. In the saturated regime, the order of such a graph is [22, 23]

$$\frac{1}{g^2} \times g^{\#\text{ of produced gluons}} \times g^{2(\#\text{ of loops})} \;, \tag{2}$$

which does not depend on the number of times the external source J is inserted into the graph. The loop expansion still corresponds to an expansion in powers of g^2, but each order in this expansion receives contributions from an infinite set of Feynman graphs that have a fixed number of loops but differ in how many sources J they contain.

Consider an observable that depends on the gluon field operator, $\mathcal{O}[\widehat{A}(x)]$ (an example could be the energy momentum tensor carried by the gluons produced in the collision). At leading order in g^2, one can show that this observable is expressible in terms of retarded classical solutions of the classical field equations of motion,

$$\langle 0_{\rm in}|\mathcal{O}[\widehat{A}(x)]|0_{\rm in}\rangle_{\rm LO} = \mathcal{O}[\mathcal{A}(x)] \;, \tag{3}$$

where

$$\left[\mathcal{D}_\mu, \mathcal{F}^{\mu\nu}\right] = J^\nu \quad , \quad \lim_{x^0\to-\infty} \mathcal{A}^\mu(x) = 0 \;. \tag{4}$$

The solution of the classical Yang-Mills equations sums the infinite series of tree graphs represented in the figure 5, where the black dots represent the external source J (only cubic vertices are represented, but in Yang-Mills theory there is also a quartic vertex). The retarded boundary condition stating that the field must vanish in the remote past is

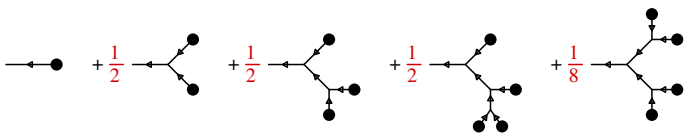

Figure 5. The first few terms in the solution of the classical equation of motion.

related to the fact that the initial state is the vacuum. The derivation of the observable in the Schwinger-Keldysh formalism provides a more rigorous justification of this boundary condition. In practical uses in heavy ion collisions, one can solve analytically the classical Yang-Mills equations up to the forward light-cone (i.e. in the regions 0, 1 and 2 of the

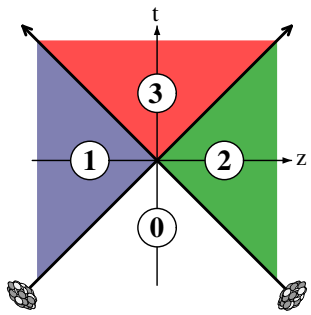

Figure 6. Division of space-time in four regions. Region 0 and empty. Regions 1 and 2 are causally disconnected and describe a single nucleus. Only region 3 contains information about the collision.

figure 6 [24]), i.e. the hypersurface where the proper time is $\tau = 0^+$ [25]. Beyond this time (i.e. in the region 3 in the figure 6), the analytical solution is not known, but it is straightforward to solve the equations of motion numerically by discretizing space on a lattice (time remains a continuously varying variable) [26–35].

3. Factorization of the distributions of sources, Color Glass Condensate

The calculation at leading order of the energy-momentum tensor of the system after the collision already provides some insight on the energy density released in the collision. However, the LO predictions for the pressure tensor are more problematic. Immediately after the collision, the longitudinal pressure is exactly the opposite of the energy density, because the chromo-electric and magnetic field lines are parallel to the collision axis [36]. At later times, the longitudinal pressure at LO always remains much smaller than the transverse pressure [36, 37], which if taken at face value would cast some doubts about the applicability of hydrodynamics to describe the bulk evolution of the system.

The hope to find large corrections at next-to-leading order, and therefore alter this pessimistic conclusion, is the main motivation to go beyond the leading order. At one loop, one encounters in fact two types of large corrections. The first one (the second type of large corrections, related to the Weibel instability, will be discussed in the next section) is made of contributions that contain logarithms of the cutoff Λ that separates the fast and the slow partons [38]. Λ enters in 1-loop corrections as the upper bound on the longitudinal loop momentum, necessary in order to avoid double counting the fast modes that are already described as external sources. The resummation of these large logarithms, that we shall describe in this section, promotes the McLerran-Venugopalan model into a full-fledged effective theory called the Color Glass Condensate[1].

The first step is to obtain a formula for the NLO corrections. For the expectation value of any inclusive observable, the NLO contribution can be written as follows [43, 44]

$$\left\langle 0_{\rm in}\middle|\mathcal{O}[\widehat{A}(x)]\middle|0_{\rm in}\right\rangle_{\rm NLO} = \left[\int_{\boldsymbol{u}} \boldsymbol{\alpha}(\boldsymbol{u})\mathbb{T}_{\boldsymbol{u}} + \frac{1}{2}\int_{\boldsymbol{uv}} \boldsymbol{\Gamma}_2(\boldsymbol{u},\boldsymbol{v})\mathbb{T}_{\boldsymbol{u}}\mathbb{T}_{\boldsymbol{v}}\right]\mathcal{O}[\mathcal{A}(x)]\ . \tag{5}$$

[1]For more detailed reviews of the Color Glass Condensate, one can consult Refs. [39–42].

The integrations are over the space-like surface where the initial conditions for $\mathcal{A}$ are set, and $\boldsymbol{\alpha}$ and $\boldsymbol{\Gamma}_2$ are 1- and 2-point functions, evaluated on this surface, that can be computed in perturbation theory. The operator $\mathbb{T}_{\boldsymbol{u}}$ is the generator of shifts of the value of the classical field at the point $\boldsymbol{u}$ on this surface (roughly speaking, $\mathbb{T}_{\boldsymbol{u}} = \delta/\delta\mathcal{A}_{\rm init}(\boldsymbol{u})$). One can understand pictorially the action of this operator in the figure 7. The left diagram

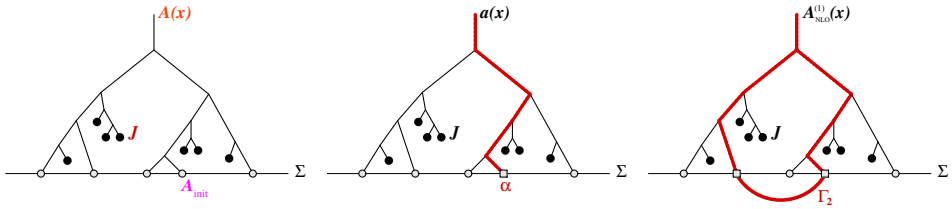

Figure 7. Illustration of the action of the shift operator $\mathbb{T}_{\boldsymbol{u}}$.

shows that the dependence of the classical field $\mathcal{A}(x)$ on its initial condition has a tree structure. In the middle diagram, we see that by replacing at one point the initial field $\mathcal{A}_{\rm init}$ by some quantity $\boldsymbol{\alpha}$ (this is what the operator $\boldsymbol{\alpha}(\boldsymbol{u})\mathbb{T}_{\boldsymbol{u}}$ does), one generates the retarded propagator that connects the points $\boldsymbol{u}$ and x, fully dressed by the background classical field. In the diagram on the right, we see that by acting with $\boldsymbol{\Gamma}_2(\boldsymbol{u},\boldsymbol{v})\mathbb{T}_{\boldsymbol{u}}\mathbb{T}_{\boldsymbol{v}}$, one generates a loop correction to the classical field. These considerations, plus a little bookkeeping, are the basis of eq. (5).

In eq. (5), the space-like surface on which the initial fields are set can be chosen at will, and the left hand side is independent of this choice. In order to extract the large logarithms that arise at NLO, it is convenient to choose a surface located just above the past light-cone (i.e. the wedge made of the lower borders of the regions 1 and 2 in the figure 6). With this choice, one can determine the logarithms analytically [43–45]:

$$\int_{\boldsymbol{u}} \boldsymbol{\alpha}(\boldsymbol{u})\mathbb{T}_{\boldsymbol{u}} + \frac{1}{2}\int_{\boldsymbol{uv}} \boldsymbol{\Gamma}_2(\boldsymbol{u},\boldsymbol{v})\mathbb{T}_{\boldsymbol{u}}\mathbb{T}_{\boldsymbol{v}} = \log(\Lambda)\Big[\mathcal{H}_1 + \mathcal{H}_2\Big] + \text{terms w/o logs} \tag{6}$$

where $\mathcal{H}_1$ and $\mathcal{H}_2$ are operators known as the JIMWLK Hamiltonians [46–54] for the two nuclei. A remarkable feature of eq. (6) is that the coefficient of the logarithms does not contain terms mixing the sources of the two nuclei. Instead, it is nicely arranged as the sum of two terms, one for each nucleus. It is this absence of mixing that allows these logarithms to be absorbed into separate distributions of sources for the nucleus 1 and the nucleus 2, respectively. Schematically, the leading log terms $(\alpha_s \log\Lambda)^n$ (i.e. at each order in α_s, the terms that have the maximal number of logarithms) can be resummed in formulas such as

$$\big\langle 0_{\rm in}\big|\mathcal{O}[\widehat{A}(x)]\big|0_{\rm in}\big\rangle_{\rm Leading\ Log} = \int [DJ_1\,DJ_2]\; W[J_1]\,W[J_2]\,\mathcal{O}[\mathcal{A}_{J_{1,2}}(x)]\;, \tag{7}$$

where $\mathcal{A}_{J_{1,2}}$ is the classical solution of the Yang-Mills equations with sources $J_{1,2}$, and the $W[J_{1,2}]$ are the probability distributions for each projectile. The latter obey the JIMWLK equation that drives their rapidity evolution :

$$\frac{\partial W}{\partial Y} = \mathcal{H}\,W\;. \tag{8}$$

The possibility to factorize these logarithms into distributions that describe the color

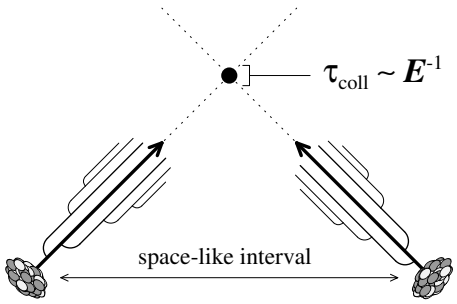

Figure 8. Causality argument for the factorization of the logarithms.

content of the two projectiles can be understood qualitatively from a simple causality argument, illustrated in the figure 8. The logarithms come from soft gluon radiation, which can only occur over long time-scales, and not during the collision itself, whose duration is very short (inversely proportional to the collision energy). For this reason, these gluons must be produced (long) before the collision, at a time when the two nuclei where not yet in causal contact. This explains why the coefficients of the logarithms cannot mix the sources of the two projectiles.

4. Instabilities, Resummation

The terms that are logarithmic in the cutoff Λ are not the only large corrections one should worry about at NLO. In order to see that, it is useful to have in mind the following representation for the 2-point function $\boldsymbol{\Gamma}_2(\boldsymbol{u},\boldsymbol{v})$ that enters in eq. (5) :

$$\boldsymbol{\Gamma}_2(\boldsymbol{u},\boldsymbol{v}) = \int \frac{d^3\boldsymbol{k}}{(2\pi)^3 2k}\, \boldsymbol{\alpha}_{\boldsymbol{k}}(\boldsymbol{u})\boldsymbol{\alpha}^*_{\boldsymbol{k}}(\boldsymbol{v}) \ , \tag{9}$$

where $\boldsymbol{\alpha}_{\boldsymbol{k}}(x)$ obeys the linearized classical equation of motion around the classical solution $\mathcal{A}$, and whose initial condition in the remote past is a plane wave of momentum $\boldsymbol{k}$. In other words, the $\boldsymbol{\alpha}_{\boldsymbol{k}}$ form a complete basis for the vector space of linear perturbations around the classical solution $\mathcal{A}$. Note that the modes that give the logarithms of Λ are those that are independent of the rapidity η.

As we shall see, large corrections to the observable can also arise from some of the modes that depend on rapidity. From the definition of the shift operator $\mathbb{T}_{\boldsymbol{u}}$, we also know that

$$\left[\int_{\boldsymbol{u}} \boldsymbol{\alpha}_{\boldsymbol{k}}(\boldsymbol{u})\mathbb{T}_{\boldsymbol{u}}\right] \mathcal{A}(x) = \boldsymbol{\alpha}_{\boldsymbol{k}}(x) \ .$$

The loop expansion of observables is based on the assumption that the mode functions $\boldsymbol{\alpha}_{\boldsymbol{k}}(x)$ remain small at all times. If for some $\boldsymbol{k}$, the perturbation $\boldsymbol{\alpha}_{\boldsymbol{k}}(x)$ becomes as large as g^{-1}, then the NLO corrections can be as large as the LO result. It turns out that this is the case for Yang-Mills equations, that are known to exhibit chaotic behavior at the classical level [37, 55–63]. The fact that their solutions are exponentially sensitive to the initial conditions means that the linearized equations of motion have some mode

functions that grow exponentially with time. In fact, these instabilities of the solutions of the classical equations of motion are closely related to the Weibel instability in anisotropic Yang-Mills plasmas [64–85]. If a mode function $\boldsymbol{\alpha}_{\boldsymbol{k}}$ grows exponentially as $\exp(\mu_{\boldsymbol{k}} t)$, then it gives a term that grows like $\exp(2\mu_{\boldsymbol{k}} t)$ in the NLO correction to the observable[2]. One can see the effect of these instabilities in the calculation of the pressure in a ϕ^4 scalar field theory (that also has unstable classical solutions for certain $\boldsymbol{k}$-modes) in the figure 9. The NLO correction is a very small correction at the beginning of the time evolution, but

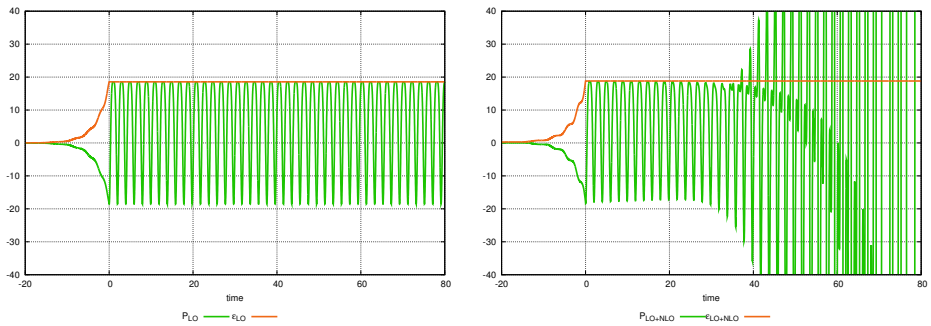

Figure 9. Example of secular divergence due to instabilities in the classical equations of motion, for the pressure in a ϕ^4 scalar field theory [86].

it grows exponentially with time. At late times, the loop expansion breaks down and one should seek a resummation that will collect and resum these large corrections. The first step in doing this is to improve the power counting in order to keep track of the growth rate of each contribution. How to do this is illustrated in the figure 10. The standard power

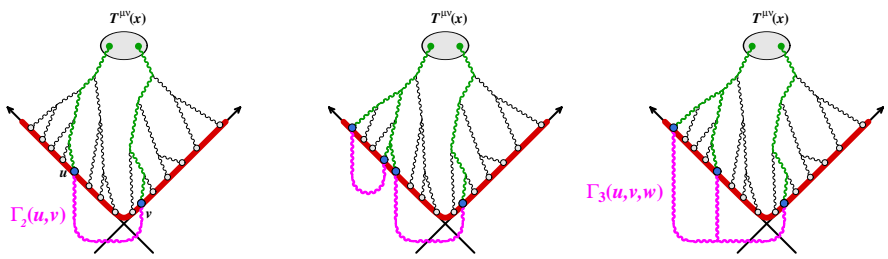

Figure 10. Loop corrections to the energy-momentum tensor.

counting (see the eq. (2)) indicates that one gets a power of g^2 for each loop. From the above discussion, one may also get an exponentially growing factor for each operator $\mathbb{T}$. From the examples of the figure 10, we see that diagrams with n loops can have up to $2n$ insertions of the operator $\mathbb{T}$, and that this maximum is reached only when the loops are independent below the surface used as initial Cauchy surface. From this observation, it appears that one can resum to all loop orders the contributions that have the fastest growth

[2]Note that the term in $\boldsymbol{\alpha}(\boldsymbol{u})\mathbb{T}_{\boldsymbol{u}}$ in eq. (5) cannot lead to a similar problem. Indeed, the 1-point function $\boldsymbol{\alpha}(\boldsymbol{u})$ is rapidity independent, and boost invariant mode functions are stable.

by exponentiating the term in $\mathbb{T}_{\boldsymbol{u}}\mathbb{T}_{\boldsymbol{v}}$ in eq. (5) :

$$\left\langle 0_{\rm in}\middle|\mathcal{O}[\widehat{A}(x)]\middle|0_{\rm in}\right\rangle_{\rm resummed} = \exp\left[\frac{1}{2}\int_{\boldsymbol{uv}} \boldsymbol{\Gamma}_2(\boldsymbol{u},\boldsymbol{v})\mathbb{T}_{\boldsymbol{u}}\mathbb{T}_{\boldsymbol{v}}\right]\mathcal{O}[\mathcal{A}(x)]\ . \quad (10)$$

(At this point, we assume that the leading logs in the cutoff Λ have already been taken care of. Not double counting these contributions is ensured by excluding the rapidity independent modes in $\boldsymbol{\Gamma}_2(\boldsymbol{u},\boldsymbol{v})$ in eq. (10).) The right hand side of this equation is not easy to evaluate in this form, but it is equivalent to letting the initial condition of the classical field $\mathcal{A}$ fluctuate with a Gaussian distribution of variance $\boldsymbol{G}(\boldsymbol{u},\boldsymbol{v})$. More precisely, we have

$$\left\langle 0_{\rm in}\middle|\mathcal{O}[\widehat{A}(x)]\middle|0_{\rm in}\right\rangle_{\rm resummed} =$$
$$= \int [D\boldsymbol{\chi}(\boldsymbol{u})]\ \exp\left[-\frac{1}{2}\int_{\boldsymbol{uv}} \boldsymbol{\Gamma}_2^{-1}(\boldsymbol{u},\boldsymbol{v})\boldsymbol{\chi}(\boldsymbol{u})\boldsymbol{\chi}(\boldsymbol{v})\right]\mathcal{O}[\mathcal{A}[\mathcal{A}_{\rm init}+\boldsymbol{\chi}](x)]\ , (11)$$

where the notation $\mathcal{A}[\mathcal{A}_{\rm init}+\boldsymbol{\chi}](x)$ denotes the value at the point x of the classical solution whose initial condition is $\mathcal{A}_{\rm init}+\boldsymbol{\chi}$ ($\mathcal{A}_{\rm init}$ being the initial condition of the classical field at LO). This alternative form of the resummed observable can be evaluated by performing a Monte-Carlo average of classical solutions that have Gaussian distributed initial conditions. It is important to note that the variance $\boldsymbol{\Gamma}_2(\boldsymbol{u},\boldsymbol{v})$ of the fluctuating initial conditions is not arbitrary: it is the same function that enters in the representation (5) of the NLO result. This means that one should first perform a 1-loop calculation in order to obtain it. This Gaussian average has also been derived in different approaches and contexts [87–91].

Given its origin as the exponentiation of the 1-loop result, this resummation contains by construction the complete LO and NLO contributions (for the latter, this is true only if one uses the variance $\boldsymbol{G}(\boldsymbol{u},\boldsymbol{v})$ given by the 1-loop calculation), and a subset of all the higher orders. The possibility to include all NLO effects solely by altering the initial conditions while keeping the time evolution classical is an example of the general property that quantum corrections to the time evolution arise only at NNLO and beyond. Order $\hbar$ corrections in the initial state come from the uncertainty principle: the fields and their conjugate momenta cannot be known simultaneously with absolute accuracy, and their distribution in phase-space must have a support of area at least $\hbar$ for each mode.

It is easy to see why this resummation cures the problem of secular divergences that plagues fixed loop order calculations. Indeed, since the resummation has promoted linearized fluctuations to fields that obey the full non-linear equation of motion, and since the potential is bounded from below (for a theory that has a well defined ground state), the fields that enter in the evaluation of the resummed observable cannot run away and generate large contributions.

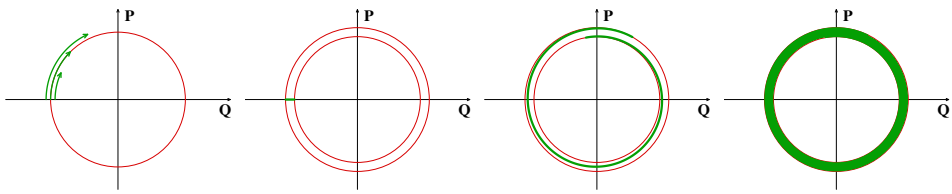

Figure 11. Illustration of the decoherence that occurs with non-linear interactions.

In the presence of non-linear interactions, one can foresee without any extensive computation that the resummed result may evolve towards some form of statistical equilibrium state. This is illustrated in the figure 11, for a single non-harmonic oscillator mode. The left figure shows that the oscillation frequency depends on the amplitude of the oscillations for such an oscillator. The 2nd, 3rd and 4th figures (from left to right) then illustrate the time evolution of an initially narrow Gaussian distribution in phase-space. The non-harmonicity will cause this distribution to stretch around the classical orbits, since the outer points rotate at a frequency that differs from that of the inner points. Eventually, the distribution covers uniformly the area allowed by energy conservation, which one may view as a micro-canonical equilibrium distribution (i.e. a distribution for which all the micro-states allowed by energy conservation are equally likely).

In order to apply this resummation to heavy ion collisions, we need to determine the variance $\boldsymbol{\Gamma}_2(\boldsymbol{u},\boldsymbol{v})$ of the spectrum of fluctuations. From this spectrum, one will then generate random initial conditions and solve numerically the classical Yang-Mills equations. For practical reasons, the numerical resolution of the equations of motion is started after the collision, at a small but positive proper time. Because of this, it is necessary to have analytical expressions for the initial background field and for the variance of the fluctuating part. The background field at $Q_s\tau \ll 1$ is already known analytically [25]. In order

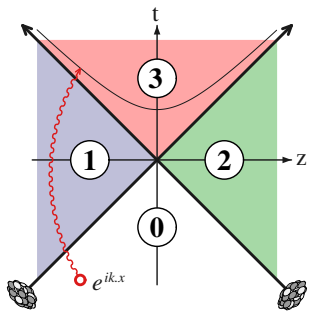

Figure 12. Evolution of a perturbation on top of the classical background field.

to calculate the variance, we use the representation of eq. (9), which reduces the problem to solving the linearized equation of motion for small perturbations to the classical background field, with a plane wave initial condition at $x^0 = -\infty$ (i.e. a mode with fixed initial momentum, color, and polarization). This calculation is illustrated in the figure 12. In order to be used as initial conditions for the Yang-Mills equations, we need these mode functions in the same gauge as the one used when solving numerically the equations, usually the Fock-Schwinger gauge $\mathcal{A}^\tau = 0$. The propagation of the perturbation over the region 0 is of course trivial, since the background field is zero there. The crossings of the light-cones (where the sources of the two nuclei are located) are a bit more delicate, because the background field has an infinite field strength there – this produces a finite jump of the fluctuation while crossing the light-cones. Finally, the propagation in the regions 1 and 2 are rather simple, because the background field is a pure gauge in these regions. On the proper time surface located at $Q_s\tau \ll 1$, the perturbation of momentum $\boldsymbol{k}_\perp, \nu$ (ν

is the Fourier conjugate of the rapidity η), color c and polarization λ reads [92]

$$\boldsymbol{\alpha}^i_{\nu\boldsymbol{k}_\perp c\lambda} = \beta^{+i}_{\nu\boldsymbol{k}_\perp c\lambda} + \beta^{-i}_{\nu\boldsymbol{k}_\perp c\lambda}\,, \qquad \boldsymbol{e}^i_{\nu\boldsymbol{k}_\perp c\lambda} = -i\nu\Big(\beta^{+i}_{\nu\boldsymbol{k}_\perp c\lambda} - \beta^{-i}_{\nu\boldsymbol{k}_\perp c\lambda}\Big)$$
$$\boldsymbol{\alpha}^\eta_{\nu\boldsymbol{k}_\perp c\lambda} = \mathcal{D}^i\Big(\frac{\beta^{+i}_{\nu\boldsymbol{k}_\perp c\lambda}}{2+i\nu} - \frac{\beta^{-i}_{\nu\boldsymbol{k}_\perp c\lambda}}{2-i\nu}\Big)\,, \quad \boldsymbol{e}^\eta_{\nu\boldsymbol{k}_\perp c\lambda} = -\mathcal{D}^i\Big(\beta^{+i}_{\nu\boldsymbol{k}_\perp c\lambda} - \beta^{-i}_{\nu\boldsymbol{k}_\perp c\lambda}\Big)\,, \tag{12}$$

(the $\boldsymbol{e}$'s are the electrical fields associated to the $\boldsymbol{\alpha}$'s) where we denote

$$\beta^{+i}_{\nu\boldsymbol{k}_\perp c\lambda} \equiv e^{\frac{\pi\nu}{2}}\Gamma(-i\nu)e^{i\nu\eta}\mathcal{U}_1^\dagger(\boldsymbol{x}_\perp)\int_{\boldsymbol{p}_\perp} e^{i\boldsymbol{p}_\perp\cdot\boldsymbol{x}_\perp}\,\widetilde{\mathcal{U}}_1(\boldsymbol{p}_\perp+\boldsymbol{k}_\perp) \times\Big(\frac{p_\perp^2\tau}{2k_\perp}\Big)^{i\nu}\Big(\delta^{ij} - 2\frac{p_\perp^i p_\perp^j}{p_\perp^2}\Big)\epsilon^j_\lambda\,, \tag{13}$$

and

$$\beta^{-i}_{\nu\boldsymbol{k}_\perp c\lambda} \equiv e^{-\frac{\pi\nu}{2}}\Gamma(i\nu)e^{i\nu\eta}\mathcal{U}_2^\dagger(\boldsymbol{x}_\perp)\int_{\boldsymbol{p}_\perp} e^{i\boldsymbol{p}_\perp\cdot\boldsymbol{x}_\perp}\,\widetilde{\mathcal{U}}_2(\boldsymbol{p}_\perp+\boldsymbol{k}_\perp) \times\Big(\frac{p_\perp^2\tau}{2k_\perp}\Big)^{-i\nu}\Big(\delta^{ij} - 2\frac{p_\perp^i p_\perp^j}{p_\perp^2}\Big)\epsilon^j_\lambda \tag{14}$$

A generic initial condition is the sum of the background field at the initial time τ_0, and of all the mode functions $\boldsymbol{\alpha}_{\nu\boldsymbol{k}_\perp c\lambda}$, weighted by random Gaussian distributed complex numbers $c_{\nu\boldsymbol{k}_\perp c\lambda}$, normalized so that

$$\Big\langle c_{\nu\boldsymbol{k}_\perp c\lambda}\, c^*_{\nu'\boldsymbol{k}'_\perp c'\lambda'}\Big\rangle = \frac{1}{2}\delta(\nu-\nu')\delta(\boldsymbol{k}_\perp - \boldsymbol{k}'_\perp)\delta_{cc'}\delta_{\lambda\lambda'}\,. \tag{15}$$

5. Evolution after the collision

Thanks to these mode functions, one can implement numerically the resummation described in the previous section in the case of heavy ion collisions. At LO, the chromo-electric and chromo-magnetic fields are parallel to the collision axis when $Q_s\tau \ll 1$ and the corresponding longitudinal pressure is negative, opposite to the energy density, while the transverse pressure equals the energy density. At later time, the longitudinal pressure increases near zero, but remains negligible compared to the transverse pressure at all times. This can be understood if the system is nearly free streaming, as illustrated in the

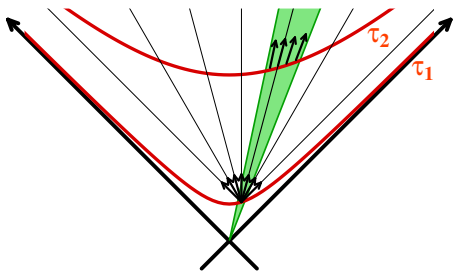

Figure 13. Evolution of the distribution of longitudinal momenta in the comoving frame for a free streaming system.

figure 13. If one starts from an arbitrary distribution of momenta at the time τ_1, and let the

particles evolve freely to the time τ_2, there will be a segregation of the local momentum distributions, such that only particles with momentum rapidity $y \approx \eta$ stay at the rapidity η. This means that the longitudinal momenta in the comoving frame are nearly zero, and the longitudinal pressure is very small.

One of the main physical issues is therefore whether the instabilities that one is resumming by including Gaussian fluctuations of the initial fields can efficiently reshuffle the momenta and compete against the longitudinal expansion of the system, in order to generate a sizable longitudinal pressure.

In order to solve numerically the classical Yang-Mills equations, one must discretize space. Moreover, one should use the $(\boldsymbol{x}_\perp, \eta, \tau)$ system of coordinates, for the boost invariance of a high energy collision to become manifest. Due to limited computational resources, one usually simulates only a small part of the collision domain, as shown in the left figure 14. The plots that will be presented later in this section have been ob-

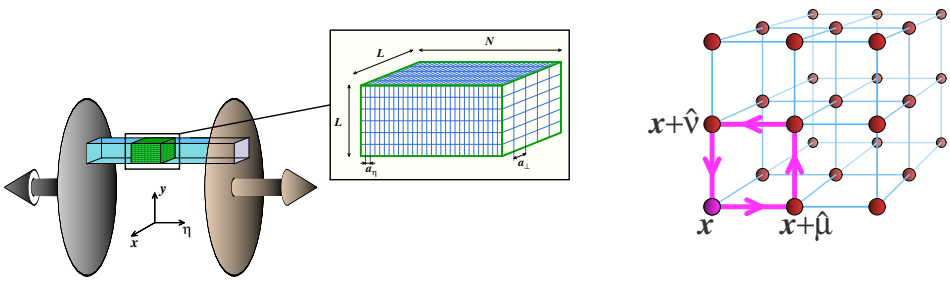

Figure 14. Lattice setup for the numerical solution of the classical Yang-Mills equations.

tained on a $64 \times 64 \times 128$ lattice (with a longitudinal lattice spacing $a_\eta = 1/64$, and a transverse lattice spacing $Q_s a_\perp = 1$) [93]. In order to preserve on the lattice an exact invariance with respect to time independent gauge transformations, the gauge potentials must be traded in favor of Wilson lines (link variables) that live on the edges of the lattice, as shown in the right figure 14. The electrical fields, that transform covariantly under these gauge transformations, live on the nodes of the lattice. In this representation, the classical Hamiltonian is a sum of the squares of the electrical fields, and of the traces of the plaquettes (product of link variables along a closed loop) that span the elementary squares of the lattice (see the figure 14).

The equations of motion are solved with the leapfrog algorithm, with time steps that are adjusted in order to conserve Gauss's law to very good accuracy. From the solution of the Yang-Mills equations, we compute the components of the energy-momentum tensor. By construction, we have

$$2P_{_T} + P_{_L} = \epsilon \; . \tag{16}$$

The energy density and longitudinal pressure are also related by Bjorken's law,

$$\frac{\partial \epsilon}{\partial \tau} + \frac{\epsilon + P_{_L}}{\tau} = 0 \; , \tag{17}$$

which arises as a consequence of local energy and momentum conservation for a boost invariant system.

A crucial step in this numerical calculation is the subtraction of the terms that would be singular in the continuum limit (i.e. in the ultraviolet). The most singular terms come

from the zero point energy, that produce a quartic divergence in the energy-momentum tensor. These terms do not depend on the background, and can be removed by performing the calculation a second time with $Q_s \equiv 0$. However, this procedure is made difficult by the fact that the ultraviolet cutoff on longitudinal momentum p_z is time dependent ($p_z^{\max} \sim a_\eta/\tau$) on a lattice with a fixed spacing in the rapidity η. Therefore, the terms that should be subtracted become very large at small τ. Since their accuracy is limited by the statistics used in the Monte-Carlo average over the initial field fluctuations, the statistical errors in the difference are large at small times.

After the zero point energy has been subtracted, the energy-momentum tensor (a dimension 4 operator) can also mix with dimension 2 operators to produce a weaker quadratic ultraviolet divergence. In the continuum, there is no local gauge invariant dimension 2 operators in Yang-Mills theory, with which it could mix. At finite lattice spacing however, an operator like the trace of a plaquette could play this role, and produce terms that are quadratic in the inverse longitudinal lattice spacing (they would affect mostly the small time behavior since the longitudinal ultraviolet cutoff behaves as $1/\tau$). In fact, such terms are seen numerically, in energy density and in the longitudinal pressure (but not in the transverse pressure, which indicates that they affect only the transverse chromo-electric and chromo-magnetic fields). In order to preserve eq. (16), the counterterms in ϵ and in P_L must be the same, and Bjorken's law then tells us that this common counterterm must be of the form A/τ^2. A deeper understanding would necessary in order to compute the prefactor A from first principles, and at the moment it is simply fitted in order to eliminate the singular $1/\tau^2$ behavior in ϵ and in P_L. The following equations summarize the subtraction procedure :

$$\begin{aligned} \langle P_T \rangle_{\text{phys.}} &= \langle P_T \rangle_{\substack{\text{backgd.} \\ +\text{ fluct.}}} - \langle P_T \rangle_{\substack{\text{fluct.} \\ \text{only}}} \\ \langle \epsilon, P_L \rangle_{\text{phys.}} &= \underbrace{\langle \epsilon, P_L \rangle_{\substack{\text{backgd.} \\ +\text{ fluct.}}}}_{\text{computed}} - \underbrace{\langle \epsilon, P_L \rangle_{\substack{\text{fluct.} \\ \text{only}}}}_{\text{computed}} + \underbrace{A\,\tau^{-2}}_{\text{fitted}} \ . \end{aligned} \tag{18}$$

Numerical results[3] are displayed in the figure 15, for two values of the strong coupling constant : $g = 0.1$ (left) and $g = 0.5$ (right). The curves show the time evolution of the ratios P_L/ϵ and P_T/ϵ, and the bands are a rough estimate of the statistical errors (they are very large at small times, because one needs to subtract two quantities varying as $1/\tau^2$, in order to get a result of order τ^0). The lower horizontal axis is in units of $Q_s\tau$, while the upper horizontal axis is in fm/c (the calibration of the time axis in physical units requires that one chooses the value of Q_s, here taken to be $Q_s = 2$ GeV, a typical value for heavy ion collisions at LHC energy). The dotted lines show the LO results for these two ratios. As said before, there is no significant buildup of longitudinal pressure at LO, and it remains much smaller than the transverse pressure at all times. The first thing to note is that at early times, $Q_s\tau \ll 1$, the resummed results are identical to the LO results. In fact, since the Weibel instabilities need a time $Q_s\tau \sim 1$ to develop, this was to be expected for the small values of the coupling considered here (note that this agreement is somewhat non-trivial because it relies on the proper subtraction of the ultraviolet contributions). At the smallest of the two couplings, the resummed result stays very close to the LO result at all times, and there is no significant increase of the longitudinal pressure compared to LO. At $g = 0.5$ (which corresponds to a 25-fold increase of α_s), some qualitative changes in the behavior of the longitudinal pressure become visible : at times $Q_s\tau \gtrsim 2$ it deviates significantly from the LO result and becomes comparable to the transverse

[3] A closely related study has also been performed in Refs. [94, 95]. In that work, weaker couplings, later times (in units of Q_s^{-1}), and a completely incoherent distribution of initial fields were considered.

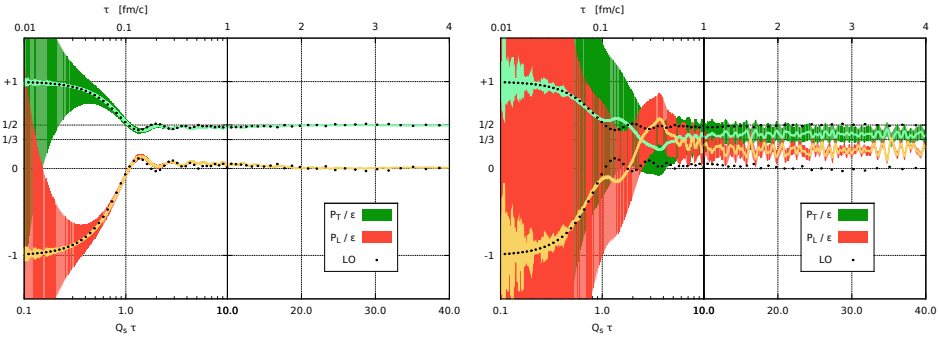

Figure 15. Time evolution of the ratios P_T/ϵ and P_L/ϵ, for $g = 0.1$ (left) and $g = 0.5$ (right). The lower horizontal axis is in units of $Q_s\tau$, and the upper horizontal axis is in fm/c, assuming the value $Q_s = 2$ GeV. The LO results are also shown for comparison.

pressure. Concomitantly, the ratio P_T/ϵ decreases from $1/2$ to a value which is much closer to $1/3$. This result suggests, that even at rather weak couplings, the higher order corrections –that involve the modes that are subject to the Weibel instability– play an important role in the isotropization of the pressure tensor.

6. Summary

In this short review, we have summarized our present understanding on how to describe the early stages of high energy heavy ion collisions in terms of quantum chromodynamics.

A central tool for these studies is the Color Glass Condensate, an effective theory for strong interactions in the regime of large gluon densities. Indeed, the gluon distribution in a hadron increases with energy due to repeated gluon emissions by bremsstrahlung. Eventually, the gluon occupation number becomes of order $1/g^2$, and the non-linear interactions among the gluons in the hadronic wavefunctions can no longer be neglected – a regime known as gluon saturation. The CGC provides a framework to study the approach to saturation, and the subsequent evolution of the gluon distribution into the saturation regime.

The CGC is also the framework of choice in order to consistently calculate the expectation value of observables after the collision of two saturated projectiles. A consequence of having large gluon occupation numbers in the two projectiles is that an infinite set of graphs contribute at each order in g^2. The leading order is given by the sum of all the tree graphs, which can be conveniently expressed in terms of solutions to the classical Yang-Mills equations. The next-to-leading order is the sum of all the 1-loop graphs, where the loop is dressed by the classical field found at leading order.

In addition to large logarithms of the collision energy (that can be absorbed into the JIMWLK evolution of the distribution of color sources), the NLO also contains secular terms, that grow exponentially with time because of the Weibel instability. It is possible to collect at each loop order the terms that have the fastest growth, and to resum them. It turns out that these contributions can all be attributed to fluctuations of the initial fields, whose time evolution remains classical. A practical way of performing this resummation is to repeat the same classical computation as the one needed at LO, with a Gaussian distribution of initial fields which is sampled with a Monte-Carlo. The variance of this

Gaussian distribution has been derived from a 1-loop calculation in [92], which paves the way for a numerical implementation of this resummation. The first numerical results implementing this program have been obtained in [93], and show that the higher order terms included via this resummation lead to an increase of the longitudinal pressure.

Acknowledgements : This work is support by the Agence Nationale de la Recherche project 11-BS04-015-01.

References

[1] F. Karsch, et al. [RBC and HotQCD Collaboration], J. Phys. **G35**, 104096 (2008).
[2] J. Adams, et al., [STAR Collaboration] Nucl. Phys. **A 757**, 102 (2005).
[3] K. Adcox, et al., [PHENIX Collaboration] Nucl. Phys. **A 757**, 184 (2005).
[4] I. Arsene, et al., [BRAHMS collaboration] Nucl. Phys. **A 757**, 1 (2005).
[5] B.B. Back, et al., [PHOBOS collaboration] Nucl. Phys. **A 757**, 28 (2005).
[6] P. Huovinen, P.V. Ruuskanen, Ann. Rev. Nucl. Part. Sci. **56**, 163 (2006).
[7] P. Romatschke, Int. J. Mod. Phys. E **19**, 1 (2010).
[8] D. Teaney, Prog. Part. Nucl. Phys. **62**, 451 (2009).
[9] P. Romatschke, U. Romatschke, Phys. Rev. Lett. **99**, 172301 (2007).
[10] F.D. Aaron, et al, [H1 and ZEUS Collaborations] JHEP **1001**, 109 (2010).
[11] A. Deshpande, R. Ent, R. Milner, CERN Courier, October 2009.
[12] L.V. Gribov, E.M. Levin, M.G. Ryskin, Phys. Rept. **100**, 1 (1983).
[13] A.H. Mueller, J-W. Qiu, Nucl. Phys. **B 268**, 427 (1986).
[14] J.P. Blaizot, A.H. Mueller, Nucl. Phys. **B 289**, 847 (1987).
[15] L.D. McLerran, R. Venugopalan, Phys. Rev. **D 49**, 2233 (1994).
[16] L.D. McLerran, R. Venugopalan, Phys. Rev. **D 49**, 3352 (1994).
[17] L.D. McLerran, R. Venugopalan, Phys. Rev. **D 50**, 2225 (1994).
[18] J. Schwinger, J. Math. Phys. **2**, 407 (1961).
[19] L.V. Keldysh, Sov. Phys. JETP **20**, 1018 (1964).
[20] R.E. Cutkosky, J. Math. Phys. **1**, 429 (1960).
[21] G. t'Hooft, M.J.G. Veltman, CERN report 73-9.
[22] F. Gelis, R. Venugopalan, Nucl. Phys. **A 776**, 135 (2006).
[23] F. Gelis, R. Venugopalan, Nucl. Phys. **A 779**, 177 (2006).
[24] Yu.V. Kovchegov, Phys. Rev. **D 54**, 5463 (1996).
[25] A. Kovner, L.D. McLerran, H. Weigert, Phys. Rev. **D 52**, 6231 (1995).
[26] A. Krasnitz, R. Venugopalan, Nucl. Phys. **B 557**, 237 (1999).
[27] A. Krasnitz, R. Venugopalan, Phys. Rev. Lett. **84**, 4309 (2000).
[28] A. Krasnitz, R. Venugopalan, Phys. Rev. Lett. **86**, 1717 (2001).
[29] A. Krasnitz, Y. Nara, R. Venugopalan, Phys. Rev. Lett. **87**, 192302 (2001).
[30] A. Krasnitz, Y. Nara, R. Venugopalan, Nucl. Phys. **A 727**, 427 (2003).
[31] T. Lappi, Phys. Rev. **C 67**, 054903 (2003).
[32] T. Lappi, Phys. Lett. **B 643**, 11 (2006).
[33] A. Krasnitz, Y. Nara, R. Venugopalan, Phys. Lett. **B 554**, 21 (2003).
[34] A. Krasnitz, Y. Nara, R. Venugopalan, Nucl. Phys. **A 717**, 268 (2003).
[35] T. Lappi, R. Venugopalan, Phys. Rev. **C 74**, 054905 (2006).
[36] T. Lappi, L.D. McLerran, Nucl. Phys. **A 772**, 200 (2006).
[37] K. Fukushima, F. Gelis, Nucl. Phys. **A 874**, 108 (2012).
[38] A. Ayala, J. Jalilian-Marian, L.D. McLerran, R. Venugopalan, Phys. Rev. **D 53**, 458 (1996).
[39] E. Iancu, R. Venugopalan, Quark Gluon Plasma 3, Eds. R.C. Hwa and X.N. Wang, World Scientific, hep-ph/0303204.
[40] T. Lappi, Int. J. Mod. Phys. **E20**, 1 (2011).
[41] H. Weigert, Prog. Part. Nucl. Phys. **55**, 461 (2005).
[42] F. Gelis, E. Iancu, J. Jalilian-Marian, R. Venugopalan, Ann. Rev. Part. Nucl. Sci. **60**, 463 (2010).

[43] F. Gelis, T. Lappi, R. Venugopalan, Phys. Rev. **D 78**, 054019 (2008).
[44] F. Gelis, T. Lappi, R. Venugopalan, Phys. Rev. **D 78**, 054020 (2008).
[45] F. Gelis, T. Lappi, R. Venugopalan, Phys. Rev. **D 79**, 094017 (2009).
[46] I. Balitsky, Nucl. Phys. **B 463**, 99 (1996).
[47] J. Jalilian-Marian, A. Kovner, L.D. McLerran, H. Weigert, Phys. Rev. **D 55**, 5414 (1997).
[48] J. Jalilian-Marian, A. Kovner, A. Leonidov, H. Weigert, Nucl. Phys. **B 504**, 415 (1997).
[49] J. Jalilian-Marian, A. Kovner, A. Leonidov, H. Weigert, Phys. Rev. **D 59**, 014014 (1998).
[50] J. Jalilian-Marian, A. Kovner, A. Leonidov, H. Weigert, Phys. Rev. **D 59**, 034007 (1999).
[51] J. Jalilian-Marian, A. Kovner, A. Leonidov, H. Weigert, Phys. Rev. **D 59**, 099903 (1999).
[52] E. Iancu, A. Leonidov, L.D. McLerran, Nucl. Phys. **A 692**, 583 (2001).
[53] E. Iancu, A. Leonidov, L.D. McLerran, Phys. Lett. **B 510**, 133 (2001).
[54] E. Ferreiro, E. Iancu, A. Leonidov, L.D. McLerran, Nucl. Phys. **A 703**, 489 (2002).
[55] P. Romatschke, R. Venugopalan, Phys. Rev. Lett. **96**, 062302 (2006).
[56] P. Romatschke, R. Venugopalan, Eur. Phys. J. **A 29**, 71 (2006).
[57] P. Romatschke, R. Venugopalan, Phys. Rev. **D 74**, 045011 (2006).
[58] T.S. Biro, C. Gong, B. Muller, A. Trayanov, Int. J. Mod. Phys. **C 5**, 113 (1994).
[59] U.W. Heinz, C.R. Hu, S. Leupold, S.G. Matinyan, B. Muller, Phys. Rev. **D 55**, 2464 (1997).
[60] J. Bolte, B. Müller, A. Schäfer, Phys. Rev. **D 61**, 054506 (2000).
[61] H. Fujii, K. Itakura, Nucl. Phys. **A 809**, 88 (2008).
[62] H. Fujii, K. Itakura, A. Iwazaki, Nucl. Phys. **A 828**, 178 (2009).
[63] T. Kunihiro, B. Muller, A. Ohnishi, A. Schafer, T.T. Takahashi, **A** Yamamoto, Phys. Rev. **D 82**, 114015 (2010).
[64] S. Mrowczynski, Phys. Lett. **B 314**, 118 (1993).
[65] S. Mrowczynski, Phys. Lett. **B 393**, 26 (1997).
[66] A.K. Rebhan, P. Romatschke, M. Strickland, Phys. Rev. Lett. **94**, 102303 (2005).
[67] A.K. Rebhan, P. Romatschke, M. Strickland, JHEP **0509**, 041 (2005).
[68] S. Mrowczynski, A. Rebhan, M. Strickland, Phys. Rev. **D 70**, 025004 (2004).
[69] P. Romatschke, M. Strickland, Phys. Rev. **D 68**, 036004 (2003).
[70] P. Romatschke, M. Strickland, Phys. Rev. **D 70**, 116006 (2004).
[71] A.K. Rebhan, D. Steineder, Phys. Rev. **D 81**, 085044 (2010).
[72] A.K. Rebhan, M. Strickland, M. Attems, Phys. Rev. **D 78**, 045023 (2008).
[73] P. Arnold, J. Lenaghan, G.D. Moore, JHEP **0308**, 002 (2003).
[74] P. Arnold, J. Lenaghan, G.D. Moore, L.G. Yaffe, Phys. Rev. Lett. **94**, 072302 (2005).
[75] P. Arnold, G.D. Moore, Phys. Rev. **D 73**, 025013 (2006).
[76] P. Arnold, G.D. Moore, Phys. Rev. **D 73**, 025006 (2006).
[77] P. Arnold, G.D. Moore, Phys. Rev. **D 76**, 045009 (2007).
[78] P. Arnold, G.D. Moore, L.G. Yaffe, Phys. Rev. **D 72**, 054003 (2005).
[79] A. Dumitru, Y. Nara, M. Strickland, Phys. Rev. **D 75**, 025016, (2007).
[80] D. Bodeker, K. Rummukainen, JHEP **0707**, 022 (2007).
[81] J. Berges, D. Gelfand, S. Scheffler, D. Sexty, Phys. Lett. **B 677**, 210 (2009).
[82] J. Berges, S. Scheffler, D. Sexty, Phys. Rev. **D 77**, 034504 (2008).
[83] A. Kurkela, G.D. Moore, JHEP **1112**, 044 (2011).
[84] A. Kurkela, G.D. Moore, JHEP **1111**, 120 (2011).
[85] M. Attems, A. Rebhan, M. Strickland, Phys. Rev. **D 87**, 025010 (2013).
[86] K. Dusling, T. Epelbaum, F. Gelis, R. Venugopalan, Nucl. Phys. **A 850**, 69 (2011).
[87] D. Polarski, A.A. Starobinsky, Class. Quant. Grav. **13**, 377 (1996).
[88] D.T. Son, hep-ph/9601377.
[89] S.Yu. Khlebnikov, I.I. Tkachev, Phys. Rev. Lett. **77**, 219 (1996).
[90] R. Micha, I.I. Tkachev, Phys. Rev. **D 70**, 043538 (2004).
[91] K. Fukushima, F. Gelis, L. McLerran, Nucl. Phys. **A 786**, 107 (2007).
[92] T. Epelbaum, F. Gelis, Phys. Rev. **D 88**, 085015 (2013).
[93] T. Epelbaum, F. Gelis, Phys. Rev. Lett. **111**, 232301 (2013).
[94] J. Berges, K. Boguslavski, S. Schlichting, R. Venugopalan, arXiv:1303.5650.
[95] J. Berges, K. Boguslavski, S. Schlichting, R. Venugopalan, arXiv:1311.3005.